1-1997

An Embedded Ring Approach to the Vibrational Dynamics of Amorphous Materials

JR Dennison
Utah State University

T. E. Doyle

Recommended Citation
JR Dennison and T. E. Doyle, "An Embedded Ring Approach to the Vibrational Dynamics of Amorphous Materials," Carbon, 35(10-11) 1465-1477 (1997).

AN EMBEDDED RING APPROACH TO THE VIBRATIONAL DYNAMICS OF LOW-DIMENSIONAL AMORPHOUS SOLIDS WITH APPLICATIONS TO GRAPHITIC CARBON MATERIALS

J. R. Dennison

Physics Department, Utah State University, Logan, UT 84322-4415

T. E. Doyle

Thiokol Corporation, Brigham City, UT 84302-0707

(Recieved 9 January, 1997; accepted 11 March, 1997)

Abstract -- A theoretical approach has been developed to model the vibrational modes of amorphous, two-dimensional materials. The method considers that the vibrational density of states is composed primarily of states originating from embedded ring structures of medium-range order. The materials are modeled as continuous random networks comprised of a statistical distribution of symmetric, planar rings with four to eight members. The rings are treated as local structural units embedded in the material, similar to molecules within a solid. The ring potentials are approximated with a valence force model (bond-stretching and bond-angle-bending force constants) modified by a third harmonic, effective force constant coupling the rings to the surrounding network. The molecular dynamics of the rings are analyzed with the use of group theory, and the frequencies are calculated using a normal coordinate treatment. The utility of the embedded ring approach lies in its use of the material's ring statistics and ring mode frequencies, allowing determination of the structure of an amorphous material from its vibrational spectrum or prediction of vibrational spectra and density of states from structural models. The method is applied here to various graphitic carbon materials as a test case and predicts a set of force constants and Raman spectra consistent with previous data and structural models.

Keywords -- Vibrational dynamics, rings, amorphous carbon, graphite, Raman spectroscopy

1. INTRODUCTION

Modeling the vibrational dynamics of amorphous materials presents a more difficult problem than that posed by crystalline materials. The presence of long-range translational order in crystals allows analytical solution of the equations of motion by introduction of the Born-von Karman periodic boundary condition [1]. In contrast, amorphous materials lack long-range order and are not amenable to the well-established analytical treatments. The aperiodicity of amorphous solids necessitates the use of statistical descriptions in structural models. As a consequence, other theoretical approaches have been developed to model the vibrational dynamics of amorphous materials [2]. A majority of these are numerical approaches. The analytical approaches developed to date can be applied only to a few specific materials and yield only qualitative results. No generalized analytical approach has yet been found to model the dynamics of amorphous materials.

This paper addresses the problem of the vibrational dynamics of 2D amorphous materials by developing an embedded ring approach (ERA), which is based upon statistical distributions of a prevalent medium-range structural unit--the planar ring. The approach is a hybrid method which uses concepts from both previous analytical and numerical methods to predict vibrational states. It embodies both the use of local dynamics (analytical approaches) and the use of mathematical techniques to account for the influence of an embrasive disordered network. The ERA is also closely related to numerical approaches, since the vibrational mode intensities in the vibrational density of states (VDOS) are directly computed from the ring statistics of a representative network cluster.

In the next section, we discuss the relation of our embedded ring approach to other methods used to determine vibrational dynamics of amorphous solids. This is followed by a detailed description of our computational methods. There we determine the in-plane vibrational modes of n=4, 5, 6, 7, and 8-membered coupled, symmetric, planar rings using Born force constants for bond-stretching and bond-angle-bending with an additional force constant used to couple the rings to the surrounding network. In Section 4, we present calculations of force constants and Raman spectra, based on structural models of various graphitic carbon materials, as a test of the ERA. In particular, we have studied graphitic amorphous carbon (g-C), which provides a simple (nearly 2D, with a single type of atom and one dominant bond type), prototypic example of a large class of continuous random network (CRN) solids in which ring or cluster vibrations cannot be fully decoupled from the network in which they are embedded. Extension of the ERA to 2D polyatomic and 3D amorphous materials is reviewed in the last section.

2. Background

Various numerical approaches attempt to predict the vibrational density of states (VDOS) for amorphous materials by considering fairly large clusters of atoms (50-1500 or more atoms) [2,3]. These approaches solve the eigenvalue problem as formulated with the use of quantum mechanics. Such approaches require some method to determine the static structure of the large cluster and often employ periodic boundary conditions. In the cluster-Bethe-lattice method [2,4,5,6], a cluster is extracted from a disordered network, and the influence of the missing embrasive network is modeled by attaching a branching structure (the Bethe lattice) onto each dangling bond at the edge of the cluster. The Bethe lattice models the influence of the missing embrasive network by eliminating the edge or surface effects which arise from plucking a finite cluster out of an infinite network. Other numerical methods (*e.g.*, equation of motion [2], recurrence [2] and quantum Monte' Carlo [7] method) have been reviewed elsewhere.

Analytical approaches examine the local dynamics of small cluster of atoms (2 to about 8 atoms) in a disordered network [2]. For bonds in such networks showing a high degree of covalency, the bond-stretching force constants typically exceed the bond-angle-bending force constants by a factor of five; t herefore, only bond-stretching forces are usually considered [2]. Vibrational frequencies are calculated for a local arrangement of atoms in the network, such as a tetrahedrally- or octahedrally-coordinated cluster of atoms. The calculations derive from simple expressions (solutions to either Lagrange's equations or Newtonian equations of motion) and relate frequency to the atomic masses, bond-stretching force

constants, and bond angles. The expressions yield bands of frequencies, with band limits determined by simple criteria and band peaks centered on non-zero vibrational modes.

The vibrational properties of materials are determined to a large extent by the local arrangement of atoms [2, 8-10]. This is especially significant for amorphous materials, which lack long-range order but display limited short-range order, and perhaps even medium-range order. Thus, one approach is to model the structure with a statistical distribution of some small number of short- or medium-ranged structures. In such an approach, a structural unit must be identified in an amorphous material to supplant the crystalline unit cell; further, one must determine the coupling between adjacent amorphous structural units in analogy to periodic boundary conditions in crystals. As an example, the lattice vibrations of crystalline silicon result primarily from the local four-coordinated tetrahedral structure of the silicon atoms. Many aspects of the dynamics of crystalline silicon can be derived from this local structure, in particular the general characteristics of the VDOS [2,8]. The local tetrahedral structure persists in amorphous silicon, with disorder resulting in a distribution of bond lengths and bond angles. By incorporating these effects of disorder in the VDOS, the dynamics of amorphous silicon have been extrapolated. The results agree qualitatively with the experimentally-determined VDOS of amorphous silicon [2,6].

The use of short-range order (local atomic arrangement) provides an analytical approach for determining the vibrational dynamics of 3D amorphous solids. The technique can be applied to 2D amorphous materials as well, once a basic, local structural unit is chosen. For 2D covalently-bonded systems, a natural local structural unit (analogous to the silicon tetrahedron) is the three-coordinated, planar arrangement of four atoms forming a triangular cluster [Figure 1(a)]. Alternately, such small clusters can be arranged to form rings of diverse sizes [Fig. 1(b)]. These larger structural elements can better model medium-range order present in 2D CRN materials and, in essence, provide a correction to Zachariasen-Warren CRN models based on short-range order [5,11]. The contribution of the ring modes of vibration to the VDOS are significant, and yet such contributions would be neglected with the use of the smaller triangular cluster as the basic unit.

Galeener [12-14] used rings as basic structural units for the analysis of amorphous solid dynamics but limited the analysis to specific vibrational modes of silica rings isolated from the random network of the glass. His analysis revealed that the sharp features in the Raman spectra of amorphous silica modes arise from the oxygen breathing modes of SiO_2 rings of various sizes which are vibrationally decoupled from the surrounding atoms, effectively isolating the ring modes from the long-range disorder. Galeener showed that vibrational decoupling of the rings is achieved by a cancellation of central forces with noncentral forces at the silicon atoms. Other silicate and borate glasses display similar ring-mode decoupling [10,11,15-19]. The sharp peaks observed in these cases are anomalies, since vibrational spectra of amorphous material generally have broad features which blend into a continuum. The broadening of features is a consequence of disorder and the relaxation or breakdown of Raman selection rules.

Although nearly complete ring-mode decoupling will occur only for a few materials of certain compositions and structures, the use of ring vibrational modes presents a fruitful approach for analytically determining the vibrational characteristics of amorphous materials [11,19]. Recently, Galeener *et al.* extended their work on decoupled rings [12-14] to ring structures in 3D CRN's which were coupled to the surrounding network using a Bethe-lattice method [5]. In contrast to amorphous silica, the ring motions in an amorphous CRN material will *in general* be coupled to the collective motions of the network. CRN's arise from the disordered arrangement of atoms or molecules with highly directional covalent bonding, resulting in a low coordination number. CRN's have been most successfully applied to covalent inorganic glasses with binary compositions. In addition to As_2Se_3 and As_2S_3, typical glass-forming binary compounds include B_2O_3, SiO_2, GeO_2, P_2O_3, As_2O_5, and As_2O_3 [20]. Figure 1(c) presents a Zachariasen schematic [20] of a CRN for an A_2B_3-type compound. The numbers of rings as a function of size are the ring statistics for the structure [Fig. 1(d)], and this distribution of n-membered rings (n=3 to about 10) provides a method of characterizing the 2D CRN. Ring statistics for real glasses are difficult to determine experimentally. However, ring statistics for vitreous SiO_2, B_2O_3, and various SiO_2-B_2O_3 glasses have been determined with the use of infrared and Raman spectra [17]. Raman spectra may also be used to determine the ring statistics for various silicate glasses [15].

Our embedded ring approach builds upon Galeener's results [12-14] by expanding upon the use of rings as structural units for vibrational modes. Instead of being limited to the specific cases of ring mode-network decoupling in some materials, we consider the more general case of ring modes coupled to a CRN. Ring modes are calculated from basic principles using techniques developed for study of molecular dynamics. A simple method is then introduced to couple the rings to the CRN. The modified mode frequencies and the ring statistics are then used to predict theoretical spectra for comparison with real vibrational spectra of materials. Indirect comparison can, thus, be made between a material's atomic structure and the model structure.

3. Methods

A ring of atoms embedded in a 2D network can be treated as a molecular entity, and methods used for determining molecular vibrations are directly amenable for determining the ring motions. Introduction of our method for coupling each ring to the network introduces the only modification required. Our use of an harmonic, effective force coupling constant is perhaps the simplest way to model the difficult problem of coupling a statistical distribution of structures to the embedding disordered network. For example, a 6-membered carbon ring in amorphous carbon can be described as a benzene-like ring embedded in a random network. The hydrogen bonds of the benzene molecule are modified to represent the effective ring-network coupling [Fig. 2(a)], which results in a modification of the ring motions and frequencies. For the dynamics of an amorphous CRN material, the in-plane vibrational frequencies for 4-, 5-, 6-, 7-, and 8-membered carbon rings have been derived to account for the distribution of ring sizes in a network [21].

3.1 Embedded ring approach model

The structural model for the ERA is constructed by extracting an n-membered ring of monatomic or polyatomic composition [Figs. 2(a) and 2(b)] from the network. The bonds joining the atoms in the ring retain the normal force constants expected for atom-atom bonding in the material. The bonds joining the ring atoms to the rigid wall, however, represent the coupling between the ring and the network. The ERA attempts to account for the effects of the network's collective motions on the ring through an effective coupling force constant, f_c. f_c then is *not* the normal atom-atom bond-stretching force constant, but a weighted force constant modified to reflect the random network's influence on the ring. The motions of the rings are then solved with the use of conventional techniques from classical mechanics, and frequencies for the modes of oscillation for each n-membered ring are extracted.

For a first-order approximation of the atomic potentials, a central force model is often employed, with only a bond-stretching force constant, f_r, and appropriate kinetic energy terms used in the calculations. The calculations are simple and straight forward, requiring only the application of the standard methods of small oscillations [22,23]. The valence force model used here provides a second-order approximation, incorporating not only f_r, but also a bond-angle-bending force constant, f_Θ. Angular kinetic energy terms are included, and the number of internal coordinates required also increases. The valence force model used here precludes the use of second and third nearest-neighbor interaction terms by imposing a rigid "wall" between the ring atoms and the random network. Limiting the ERA to a simple valence force model with only nearest-neighbor interactions presents a justifiable approximation for amorphous materials; most previous studies employ only a central force approximation [2].

The valence force model is a more accurate model than the central force model, but at the expense of quadrupling the complexity of the calculations. In addition to the two translational displacement coordinates (decoupled in the central force model), two angular coordinates are also required for each atom in the embedded ring to account for bond angle bending. This increases the total number of coordinates for the n-membered embedded ring system from 2n to 4n. Additionally, coordinate cross-product terms which vanish in the central force model do not vanish in the valence force model. Finally, the kinetic energy matrix coefficients will be different for each n-membered ring, since the bond angles differ for each n-membered ring. Consequently, the secular determinant for an n-membered ring expands from n x n for the central force model to 4n x 4n.

3.2 Determination of frequency modes

The application of group theory and the normal coordinate treatment to the ERA becomes essential when a valence force model is adopted. The utility of group theory goes beyond that of managing the calculations. It provides insights into the most probable modes of oscillation for the rings and shows the dependence of vibrational frequency on variations in bond length and force constants. By approximating the configurations of the embedded rings with planar regular polygonal shapes, full advantage can be taken of symmetry elements and their corresponding symmetry operations. (Barrio *et al.* [5] provide arguments, based on minimization of network energy, that regular rings are favored. In carbon materials, extended π-bond interactions favor planar structures [24].) The symmetry elements of a ring allow classification of the ring to a molecular symmetry point group. Vibrational species, fundamental modes, Raman active modes, and infrared active modes for the embedded rings are obtained from the character tables of their corresponding point groups [25-28].

Only in-plane vibrational modes (appropriate for the 2D systems studied here) of monatomic n-membered rings have been examined to date. The respective point groups for the 4- to 8-membered symmetric rings (regular polygons) are D_{4h}, D_{5h}, D_{6h}, D_{7h}, and D_{8h}. Table 1 lists the in-plane vibrational species, fundamentals, and Raman active fundamentals for the 4- to 8-membered rings. Each embedded ring has 2n-3 vibrational degrees of freedom in 2D (*i.e.*, 2n-3 in-plane fundamentals). Two degrees of freedom are subtracted for translation of the ring's center of mass, and one is subtracted for rigid rotation of the ring (corresponding to A_{2g} or A_2ℕ modes). The Raman active modes include the A_{1g} or A_1ℕ modes (symmetrical breathing modes) and the E_{2g} or E_2ℕ modes (elongation along an in-plane symmetry axis) which have similar motions for all sized rings. Figure 3 illustrates the fundamental, in-plane modes for 7-membered rings. Comparable figures for the other size rings are found in Doyle [21].

The secular equation, $\mathbf{V}_{i,j}-\omega^2\mathbf{T}_{i,j}=0$, where **V** and **T** are the potential and kinetic energy matrices, respectively, can alternatively be expressed as $*\mathbf{gf}-\mathbf{I}\omega^2*=0$, written in terms of internal coordinates (**I** is the identity matrix). The **f** (potential energy) matrix terms include only three force constants: f_r (corresponding to the coordinate t), f_c (corresponding to the coordinate s), and f_Θ (corresponding to the coordinates, α and β). No interaction terms are included, and the resulting **f** matrix is diagonal in form. The **g** matrix is more amenable to solution of the secular equation [23,27,28] and is related to the kinetic energy matrix by $2T = \sum_{i,j} g_{ij}\, p_i\, p_j$. Here p_i is the momentum conjugate to q_i, the i^{th} internal coordinate; the g_{ij}'s are the **g** matrix elements; and the summation is over both coordinate sets, i and j.

The internal coordinates selected for the valence force model were those used by Wilson *et al.* [23,29] in their vibrational analysis of the benzene molecule and are displayed in Fig. 2(c). The coordinates, t and s, are the atom-atom bond distance displacement and the atom-rigid wall bond distance displacement, respectively. The coordinates, α and β, are not the standard bond angle displacements but rather the change in the internal ring angle (α) and the angle between the internal ring angle bisector and the atom-rigid wall bond (β).

A further transformation was made from internal coordinates to symmetry coordinates (see Table 2) using the character tables. The value of the symmetry coordinates lies in their ability to transform the **f** and **g** matrices into factored potential energy and kinetic energy matrices [the **F** and **G** matrices in Table 3(a)]. These factored matrices allow partitioning of the original 4n x 4n secular determinant given by $*\mathbf{GF}-\mathbf{I}\omega^2*=0$ into smaller 2 x 2 and 4 x 4 secular determinants, each corresponding to a particular vibrational species. Transformation of the **f** matrices yielded diagonal **F** matrices with the force constants as the diagonal elements. Transformation of the **g** matrix yielded **G** matrices with elements comprised of linear combinations of **g** matrix elements [Table 3(b)].

The **g** matrix elements for the embedded rings were determined by the use of the vector method described by Wilson *et al*. [23]. Atomic masses, bond angles, and bond distances are used to construct the **g** matrix elements. To use the vector method, each bond is required to terminate at an atom with a given mass. A hypothetical atom with infinite mass is, therefore, placed at the outer end of the coupling bond,

since no atom exists there in the structural model for the embedded ring. The infinite mass fixes the end of the coupling bond to the rigid wall. This presents no difficulty in the **g** matrix elements because only the reciprocal of the masses appears. Some of the terms in the **g** matrix elements consequently vanish.

These secular determinants [see Table 3(c)] were solved, the roots of the resulting polynomials were obtained, and the frequencies, ω, and eigenvectors for each mode were determined. Vibrational species were assigned to each mode of oscillation by examining the symmetry operations denoted by the displacements.

4. Application to Graphitic Carbon

To study the efficacy of our embedded ring approach, we applied the method described above to the study of the Raman spectra of graphitic carbon materials. We restrict the studies here to carbon materials with almost totally sp^2 bonding, which have structures which can be described in terms of ring statistics. Vibrational (Raman) spectra were modeled using the frequencies determined from the embedded ring approach, Raman selection rules, and ring statistics for various structural models. Raman spectroscopy is an appropriate dynamical probe, as it is extremely sensitive to both medium- and short-range structural order in g-C [30].

Raman spectra of large single crystal graphite [Fig. 4(a)] exhibit a single high frequency line (E_{2g} mode) at 1581 cm^{-1}. A breakdown of Raman selection rules allows the A_{1g} mode near 1360 cm^{-1} to become Raman active in nanocrystalline graphite [Fig. 4(b)] [31,32]. The n=6 A_{1g} (abbreviated $^6A_{1g}$) and similar A_1-type modes are Raman active for isolated rings (see Table 1), so the appearance of $^6A_{1g}$ in nanocrystalline graphite is not unexpected. The broad, asymmetric Raman spectrum of g-C [Fig. 4(d)] is of a commercially available evaporated amorphous carbon sample [33] which has been well characterized [34,35] and has a Raman spectrum very similar to other published g-C spectra [30,36].

4.1 Comparison with polycyclic aromatic hydrocarbons

To determine whether local vibrational modes of 2D CRN's, such as g-C, can be modeled by studying the modes of individual rings, we examined the effects of ring coupling in a systematic fashion for symmetric benzenoid (n=6) rings by analyzing the specific mode frequencies corresponding to the A_{1g} and E_{2g} peaks of nanocrystalline graphite for 16 successively larger polycyclic aromatic hydrocarbon (PAH) molecules (Fig. 5). The graphite E_{2g} [A_{1g}] mode had atomic motion most similar to totally symmetric, Raman active, predominately bond-stretching, quinoidal-type [Kekule-type] PAH modes, based on Cartesian displacement diagrams, ring motion analysis, and potential energy distribution analysis.[37-41] These published frequencies have <2% deviation for from two to 13 rings. This demonstrates that the coupling and frequency for a nearly isolated molecular ring mode, modified by the addition of even a few surrounding carbon rings, approach values of an infinite, ordered network of 6-membered rings (graphite). That is, these frequencies are relatively insensitive to a longer-range medium-range order of ring clusters. Therefore, we expect similar frequencies for a given n-membered ring in an infinite raft of regular rings (*e.g.*, graphite), smaller structures of regular rings (*e.g.*, PAH molecules), larger (*e.g.*, Beeman's model [24]) and smaller (*e.g.*, models of Galli *et al.* [42] and Ho and coworkers [43]) quasi-2D CRN amorphous ring structures, or single rings coupled only to nearest neighbor rings (*e.g.*, the ERA).

4.2 Determination of force constants

Application of the ERA requires determining a set of force constants which approximate the covalent bonding forces for the specific 2D amorphous material and the network coupling to be studied. Both the bond-stretching and bond-angle-bending force constants can be obtained from either atomic force calculations or derived from spectroscopic measurements of crystalline compounds containing the same type of atomic bonds. The effective coupling force constant is arrived at by examining the network motions and the relative motions of the ring atoms with respect to the network atoms for each vibrational mode.

The ERA force constants applicable to g-C were determined uniquely by satisfying three constraints

based on physical intuition. The secular equations for the Raman active $^6A_{1g}$ and $^6E_{2g}$ modes were constrained to match the experimental frequencies (1360 cm^{-1} and 1581 cm^{-1}, respectively, using the Ar 2.41 eV line) of nanocrystalline graphite with a bond length of t=1.42 Å. In addition, f_c was set equal to $2f_r$.

Physically, we expect $\eta / f_c/f_r$ to be less than or equal to two. In the 6-membered ring A_{1g} and E_{2g} modes of nanocrystalline graphite (see Fig. 5), each network atom moves with the same displacement but in opposite direction to the adjacent embedded ring atom with which it is coupled. By replacing the network atom with a rigid wall, the effect of the opposing motions of the network atoms can be accommodated with an effective coupling force constant twice the bond-stretching force constant ($f_c=2f_r$). A cursory examination of 6-membered ring mode motions (with respect to network atom motions) concludes that the A_{1g}, E_{2g} and B_{1u} modes are sufficiently modeled with $f_c=2f_r$, but the B_{2u} and E_{1u} modes are not. The same coupling force constant ($f_c=2f_r$) would also be most appropriate for the n=4 A_{1g} and B_{1g} modes, the n=5 A_1ℕ mode, the n=7 A_1ℕ mode, and the n=8 A_{1g}, B_{1g} and B_{2g} modes. Relative motions for other modes suggest η#2. Deviation from symmetric or planar rings or rafts also leads to 0#η<2.

The above scenario is analogous to the 1D problem of two masses joined by a spring. The two mass-spring system, Figure 6(a), oscillates with a frequency of ω = %2k/m, and the two masses move in opposite directions, with a node at the center of mass. Placing an imaginary rigid wall at the center of mass [see Fig. 6(b)] results in a system which oscillates at a frequency of ω = %kℕ/m for which kℕ is the force constant of the spring in the new system. To oscillate at the same frequency as the two mass-spring system, kℕ = 2k. In the embedded ring system, k corresponds to f_r, and kℕ corresponds to f_c. Therefore, $f_c=2f_r$ to accurately accommodate the effect of the network on the motions on the embedded ring.

The three constraints yielded f_Θ/t^2=55 N/m, f_r=436 N/m, and f_c=873 N/m for graphitic carbon with t=1.42 Å. These are comparable to values reported in the literature for nearest-neighbor force constants for graphite and sp^2-bonded g-C of 25#f_Θ/t^2#267 N/m and 313#f_r#459 N/m [24,44]. Figure 7 shows the values of η for a range of values for f_r and f_Θ/t^2 subject only to the constraints to match the two experimental frequencies. When subject to the additional constraint, $f_c=\eta f_r$ (dashed line in Fig. 7), we find that for f_Θ/t^2 to be positive η>1.

Table 4 shows frequencies calculated from the ERA for all fundamental in-plane modes of the five sizes of rings (this excludes low frequency rigid translation and rotation A_2-type modes). The eleven modes which are Raman active for isolated (fully decoupled) symmetric rings are shown in italics in Table 4; these are the modes used to fit the Raman spectra of graphitic carbon below. The A and B-type modes in the valence force model result in 2 x 2 secular determinants with one non-zero root. The E-type modes have 4 x 4 secular determinants with two non-zero roots.

We have also investigated the dependence of the force constants and resulting frequencies on three parameters of interest. As discussed above, we expect 1#η#2, depending on the strength of the coupling of the rings to the surrounding network which, in turn, depends on motions for the specific mode, deviation from symmetric planar rings and rafts, bond type, and the nature of the network structure. The dependence of the Raman active A_1- and E_2-type modes on η is shown in Fig. 8(a). The bond lengths for carbon materials considered here do not deviate too much from the bond length in graphite. However, the eigenfrequencies change over even a limited range of bond lengths, as shown in Fig. 8(b). Fits *e* and *e′* [refer to Fig. 4(a) and Table 5] illustrate the effect of bond length on predicted Raman spectra. The position of the lower Raman peak (often referred to as the D-band) observed in nanocrystalline graphite and nanotubes [45] and g-C [46] has been found to vary linearly with laser excitation energy [30]. Substitution of this energy-dependant peak position in the constraining equations yields the eigenfrequencies shown in Fig. 8(c).

4.3 Raman spectra for graphitic carbon

A series of fits (see Table 5 and Fig. 4) to Raman spectra of graphitic carbon materials has been made based on the frequencies calculated from the ERA (see Table 4) and existing structural models of the

materials which include ring statistics. All these first order Raman spectra used unpolarized scattering and the Ar 2.41 eV laser line.

The fitting parameters considered were the overall intensity of the spectra, the ratio c_A/c_E of proportionality constants for A_1-type to E_2-type mode intensities, peak widths for the two mode types and, for some fits, the bond length. The fitting parameters are listed in Table 5. Fits to crystalline samples (fits *a*-*c*) use Lorentzian lineshapes with a width, Γ, resulting from finite lifetime broadening. The additional width of peaks for amorphous samples is due primarily to the distribution of bond angles for asymmetric rings of various sizes and to the sampling of non-zero-center phonons. This additional width of each mode is modeled as a Gaussian distribution in a manner similar to that used in analyzing a-SiO_2 spectra.[41] We consider two lineshapes for amorphous materials peaks, an adjustable width Gaussian lineshape and a composite lineshape with an adjustable width Gaussian convoluted with a fixed width (set to values from fit *b*) Lorentzian.

4.3.1 Crystalline graphite

Figures 4(a) and 4(b) show fits to the Raman spectrum of single crystal graphite and nanocrystalline graphite, respectively. Agreement is quite good for both spectra. This is to be expected, since the positions of these peaks were used as constraints to determine the appropriate force constants. The intensity ratio of the two peaks in Fig. 4(b) can be used to infer an in-plane coherence length of 34 Å for the nanocrystalline sample, as described in Ref. 31.

4.3.2 C_{60} Fullerene

The limitations of an embedded ring approach are fully apparent in the fit to the Raman spectrum of powdered C_{60} shown in Fig. 7(c). Again, the peak positions were determined from our calculations, and the intensities were related to the ring statistics for a C_{60} molecule. Neither the peak positions nor intensities are predicted well.

This result is not surprising. Our model fails to take into account the full symmetry of the molecule, and our coupling method is insufficient to model interaction between the rings in such a small molecule. Further, adjacent rings in C_{60} are far from planar. Vibrational dynamics of much larger fullerene cages should be modeled better by the ERA, as these concerns are reduced for larger molecules.

4.3.3 Disordered carbon

The first significant test of the use of the ERA for amorphous materials was the study of g-C commercially prepared using arc evaporation at room temperature.[33] This material has been well characterized in previous studies.[21,33-35] Figures 4(d) and 4(e) show fits to the Raman spectrum of g-C, using two prominent models of amorphous carbon which have complete trivalent bonding and provide predictions for ring statistics [24,48].

To estimate the Raman intensity from the ring statistic for g-C, we modified the integrated peak intensities with a reduced Raman weighting factor. For amorphous, disordered, and liquid materials, the frequency weighted reduced Raman intensities are approximately constant for modes within a band (*e.g.*, the A_1- or E_2-type modes) and are approximately proportional to the VDOS and, hence, (in our model) the ring statistics [2,36,49]. In this approximation, the measured intensity for a Raman peak is proportional to $I_0 N_n c_b \{[n(\omega)+1]/\omega\}$, where I_0 is the incident radiation intensity, N_n are the ring statistics for n-membered rings, c_b is a proportionality constant for band type b, the term in curly brackets is the reduced Raman weighting, and $n(\omega)=[\exp(S\omega/k_bT)-1]^{-1}$ is the Bose occupation factor.

Predicted Raman spectra incorporating peak profiles for the Raman active A_1-type and E_2-type modes for n=5, 6, and 7, using ring statistics based on a model by Beeman *et al.* [24] as extended by Robertson,[50] produce excellent fits [Fig. 4(d)] to the measured Raman spectrum of g-C. Beeman *et al.* model g-C as a nearly 2D CRN structure, formed from 15 to 20 Å diameter nearly planar rafts, comprised of 5-,6-, and 7-membered rings (21, 59, and 21%, respectively), with very few 4- and 8-membered rings, and with little or no tetrahedral bonding. The fits shown in Fig. 4(d) and the residuals shown in Figs. 9(a) and 9(b) demonstrate that the composite Gaussian/Lorentzian lineshape produces fits superior to those using simple

Gaussian lineshapes.

Fits shown in Fig. 4(e) are based on an alternate theoretically predicted model of g-C with negative curvature in a random schwarzite structure.[48] This model does not provide as good a fit as the Beeman model, especially in the region of the spectrum from 1200 to 1400 cm^{-1}. Fits *e* and *e'* use the bond lengths predicted in Ref. 48 and that of graphite, respectively; the effect of bond length on the predicted Raman spectra is evident in the residuals shown in Figs. 9 (c) and (d).

Addition of neither n=4 and n=8 Raman active modes nor Raman inactive modes significantly improved the fits in Figs. 4(d) or (e), although it is impossible to preclude small contributions where these peaks overlapped the peaks listed in Table 5.[34] Inclusion of the single Raman active peak in diamond at 1332 cm^{-1} also did not improve these fits, suggesting that sp^3 bonding is not common in g-C. However, the diamond sp^3 Raman cross-section is ~50 times smaller than the sp^2 cross-section which prohibits detection of small amounts of sp^3 bonding [24,30,51].

Peak widths (FWHM) for these two fits ranged from ~200 cm^{-1} to 350 cm^{-1}. These widths are significantly broader than widths found in Raman spectra of water- and fluorine-bearing silica glasses (50-120 cm^{-1} FWHM) [41]; this is expected, since g-C rings are less isolated from the surrounding network, and the 2D nature of the g-C CRN requires a larger bond distribution (estimated as 117E"6E for g-C [24]) than the 3D silica CRN. The ratio, $c_A/c_{E,}$ was near unity, as would be expected for bands of modes with similar motion in the same region of the spectrum.

Related structural models of amorphous carbon [39,42,43] should give spectra similar to Fig. 4(d). However, these spectra can not be predicted using the ERA because ring statistics, which determine peak intensity, were not provided. The presence of appreciable sp^3-bonded carbon in these models may not significantly alter the spectra, as discussed above. Ring coupling to the network would be expected to be weaker (implying 1#η<2) for the non-planar rings in the models of Galli *et al.* [42] and Ho and coworkers [43]; a reduced η would lead to some changes in the mode frequencies [refer to Fig. 8(a)].

5. Results and discussion

No generalized analytical method exists which can calculate the vibrational density of states for an amorphous material. Although not a generalized method, the embedded ring approach lies in the middle ground between analytic approaches which typically look at isolated, small-scale structural elements and numerical approaches which have looked at the structure of larger clusters of atoms. The ERA emphasizes the medium-range structural order found in amorphous materials by investigating the dynamics of a statistical distribution of symmetric, planar rings of diverse size with an effective coupling force constant to model the effect of the embrasive network on the ring's vibrational modes. This approach uses simple, first-principle, classical methods which are easy to implement and provide a methodology for modeling the dynamics of local structures.

One can either fit the vibrational spectra using ring-size distributions from structural models, as was done in this paper, or extract ring statistics from fits to the data, as was done in Ref. [34]. Fits to Raman spectra of several forms of disordered graphitic carbon, based on previous structural models incorporating ring statistics, proved quite satisfactory. It is also relatively straightforward to model other vibrational spectra (*e.g.*, infrared and inelastic neutron scattering [52]) or match theoretical VDOS. We are presently extending ERA calculations to include out-of-plane vibrational modes for symmetric planar rings.

The ERA is most applicable to 2D covalent amorphous materials which can be modeled as continuous random networks and are characterized by their ring size distribution. Thus, the approach is applicable to a wide range of materials with scientific and technological interest. The simplest materials to study are 2D amorphous materials with monatomic composition, such as disordered graphitic carbon discussed above. These initial results suggest that the embedded ring approach has significant potential as a simple method to model the vibrational dynamics of CRN materials using rings as a medium-range structural unit,

particularly in situations that do not allow the rings to completely decoupled from their surroundings.

Additional materials need to be examined using the ERA to verify its efficacy. Two-dimensional CRN amorphous materials with polyatomic composition, such as amorphous As_2Se_3, As_2S_3, and As_2O_3, would provide additional test cases for the ERA. Layered materials with various degrees of disorder could also be investigated (*e.g.*, boron nitride, several of the metal halides and metal dichalcogenides, and the cuprate superconductors displaying oxygen vacancy disorder). In addition to 2D CRN's, the ERA should also be valid for 3D amorphous materials which contain planar rings (for example, SiO_2- and B_2O_3-based glasses). Although ring-network decoupling would occur for certain vibrational modes in these materials, other materials would not exhibit this phenomenon. Such ring-network coupling is accommodated by our introduction of a coupling force constant.

The ERA could also be extended to covalent 3D amorphous materials by examining the vibrational dynamics of polyhedra-forming atomic clusters in the 3D network [3]. The polyhedra would be 3D analogues of 2D planar rings, and modified vibrational modes for isolated polyhedra embedded into an embrasive network could be determined by the same methods as outlined in this work. Such an "embedded polyhedron approach" would have wider application and utility than the ERA, but more in-depth research on the ERA is required before undertaking extension to 3D amorphous solids.

Acknowledgments

We express our thanks to Mark Holtz, Mark Riffe, Ed McCullough, Michael Windham, Akeley Miller, Jim Wheeler, and Charles Torre for useful discussions. Raman spectra were provided by Mark Holtz and Tim Dallas at Texas Tech. Support for this work from the USU Office of Research (JRD) is gratefully acknowledged.

References

[1] Ashcroft, N. W. and Mermin, N. D., *Solid State Physics*, W. B. Saunders, Philadephia, PA. 1976, pp. 421-468, 780-783.

[2] Elliott, S. R. , *Physics of Amorphous Materials*, 2nd-edn., John Wiley & Sons, New York, NY. 1990, pp. 185-205.

[3] Elliott, S. R., *Nature*, 1991, **354,** 445-452.

[4] Jannopoulos, J.D., *J. Non-Cryst. Sol.*, 1979, **32**, 241.

[5] Barrio, R.A.,Galeener, F.L., Martinez, E. and Elliott, R.J., *Phys. Rev. B,* 1993, **48**, 15672.

[6] Barrio, R.A. , Nauruis, G.G. and Wang, C.M., *J. Non-Cryst. Sol.*, 1995 **182**, 22.

[7] McGreevy, R.L. and Pusztai, L., *Mol. Simul.*, 1988, **1**, 359; Gereben, O. and Pusztai, L., *Phys. Rev. B*, 1994, **50**, 14136; Kelires, P.C., *Phys. Rev. B*, 1993, **47**, 1829; Gilkes, K.W.R.,Gaskell, P.H. and Robertson, J., *Phys. Rev. B*, 1995, **51,** 12303.

[8] Sen, P. N. and Thorpe, M. F., *Phys. Rev. B*, 1977, **24,** 4030.

[9] Lucovsky, G. and Hayes, T. M., in *Amorphous Semiconductors*, Topics in Applied Physics, Vol. 36, ed. M. H. Brodsky, Springer-Verlag, Berlin, 1979;Lucovsky, G.,de Neufville, J. P. and Galeener, F. L. , *Phys. Rev. B*, 1974, **9**, 1591.

[10] Thorpe, M. F. and Galeener, F. L., *Phys. Rev. B*, 1980, **22,** 3078.

[11] Elliott, R., *J. Non-Cryst. Sol*., 1995, **182,** 1.

[12] Galeener, F. L. , *J. Non-Cryst. Solids*, 1982, **49,** 53

[13] Galeener, F. L. , *Solid State Commun.*, 1982, **44,** 1037.

[14] Galeener, F. L., Barrio, R. A., Martinez, E., and Elliott, R. J., *Phys. Rev. Lett.*, 1984, **53**, 2429.

[15] Sharma, S. K. , Mammone, J. F. , and Nicol, M. F., *Nature*, 1981, **292,** 140.

[16] Sharma, S. K. and Simons, B. , *American Mineralogist*, 1981, **66,** 118.

[17] Bell, R. J. , Carnevale, A. , Kurkjian, C. R. , and Peterson, G. E. , *J. Non-Cryst. Solids*, 1980, **35 & 36**, 1185.

[18] Windisch, C. F. and Risen, W.M., *J. Non-Cryst. Sol.*, 1982, **48,** 307 .

[19] Kerner, R., *J. Non-Cryst. Sol*., 1995, **182**, 9.
[20] Zachariasen, W. H., *J. Am. Chem. Soc.* , 1932, **54,** 3841-3851.
[21]Doyle, T. E., An embedded ring approach to the vibrational dynamics of disordered two-dimensional materials, M.S. thesis. Utah State University, Logan, UT, 1992.
[22] Goldstein, H., *Classical Mechanics*, 2nd-edn , Addison-Wesley, Reading, MA. 1980, pp. 243-274.
[23] Wilson, Jr., E. B. , Decius, J. C., and Cross, P. C., *Molecular Vibrations*, Dover, New York, NY. 1955.
[24] Beeman, D., Silverman, J., Lynds, R. and Anderson, M.R., *Phys. Rev. B*, 1984 **30,** 870.
[25] Douglas, B. E. and Hollingsworth, C. A., *Symmetry in Bonding and Spectra* ,Academic Press, Orlando, FL. 1985,.
[26] Harris, D. C. and Bertolucci, M. D., *Symmetry and Spectroscopy*, Oxford University Press, New York, NY. 1978.
[27] Ferraro, J. R. and Ziomek, J. S., *Introductory Group Theory*, Plenum Press, New York, NY. 1969.
[28] Woodward, L. A. , *Introduction to the Theory of Molecular Vibrations and Vibrational Spectroscopy*, Oxford University Press, London, 1972.
[29] Wilson, Jr, .E. B., Phys. Rev., 1934, **45**, 706..
[30] Dennison, J.R., Holtz, M. and Swain, G., *Spectroscopy*, 1996, **11**(8), 38.
[31] Tunistra F. and. Koenig, J.L, *J. Chem. Phys.*, 1970, **53,** 1126.
[32] Dillon, R.O. , Woollam, J.A., and Katkanant, V., *Phys. Rev. B*, 1984, **29,** 3482.
[33] Stoner, Jr., J.O., *J. Appl. Phys.*, 1969, **40,** 707.
[34] Doyle, T. E. and Dennison , J. R., *Phys. Rev B*, 1995, **51,** 196.
[35] Ritter, A.L. , Dennison, J.R., and Jones, R. , *Phys. Rev. Lett.*, 1984, **53**, 2054.
[36] Lannin J.S., *Phys. Rev. B*, 1977, **15,** 3863; Wada N., *J. Non-Cryst. Sol*., 1980, **53**, 543.
[37] Cyvin, B.N. and Cyvin, S.J. , *Spec. Lett.*, 1986, **19,** 1161..
[38] Ohno, K. , *J. Mol. Spectrosc.*, 1979, **77,** 329; *J. Chem. Phys.*, 1991, **95,** 5524.
[39] Cyvin, S.J., *et al., Z. Naturforsch.*, 1979, **34a** , 876; *ibid.*, 1982, **37a**, 1359.
[40] (a) Fonti, C., *et al., Infrared Phys.*, 1990, **30**, 19; (b) Schettino, V., *J. Mol. Spectrosc.*, 1970, **34,** 78; (c) van Hare, D.R., *et al., Appl. Spectrosc.* , 1984, **38,** 543; (d) Bridge, M.J. and Vincent, D. , *J. Chem. Soc. Faraday Trans. 2*, 1972, **68**(9), 1522.
[41] Mysen, B.O. and Virgo, D., in *Advances in Materials Research II*, ed. Snyder, R.L., Condrate, Sr., R.A. and Johnson, P.F. ,Plenum Press, New York, NY. 1985, pp. 43-55.
[42] Galli, G., *et al*, *Phys. Rev. Lett.* 1989, **62**, 555.
[43] Wang, C.Z. and. Ho, K.M, *Phys. Rev. Lett.*, 1993, **71,** 1184 ; Wang , C.Z.,. Ho, K.M and Chan ,C.T., *Phys. Rev. Lett.*, 1993, **70**, 611; *Phys. Rev. B*, 1992, **46**, 7333.
[44] Nicklow, R., Wakabayashi, N., and Smith, H.G. , *Phys. Rev B*, 1972, **5,** 4951; Al-Jishi, R. and Dresselhaus, G., *Phys. Rev. B*, 1982, **26**, 4514; Young, J.A. and Koppel, J.V., *J. Chem. Phys.*, 1965, **42,** 357; Kesavasamy K. and Krishnamurthy N., *Ind. J. Pure and Appl. Phys.*, 1979, **17,** 73
[45] Wang, Y., *et al., Chem. Mater.*, 1990, **2,** 557; Yoshikawa , M., *et al. Solid State Comm.*, 1988, **66**, 1177; Denisov, D. *et al., Sov. Phys. JTEP*, 1992, **75,** 158.
[46] Dallas, T., Structural phases of disordered carbon materials. Ph.D. thesis, Texas Tech Univer. Lubbock, TX,, 1996; Dallas, T. , Holtz, M., and Dennison, J.R., *Bull. Am. Phys. Soc.*, 1995, **40**,1,, 538.
[47] Zhang, Q.-M., Yi, J.-Y. and Bernhole, J., *Phys. Rev. Lett.*, 1991, **66**, 2633.
[48] Vanderbilt, D. and Tersoff, J., *Phys. Rev. Lett.*, 1992, **68,** 511; Lenosky, T., Gunze, X. , Teter ,M. and Elser, V., *Nature*, 1992, **355,** 333.
[49] Shuker, R. and Gammon, R.W. , *Phys. Rev. Lett.*, 1970, **25**, 222.
[50] Robertson, J., *Adv. Phys.*, 1986, **35**, 317.
[51] Wada, N., Gaczi, P.J. and. Solin, S.A, *J. Non-Cryst. Sol.*, 1980, **35&36,** 543.
[52] Doyle, T.E. and Dennison, J.R., (unpublished).

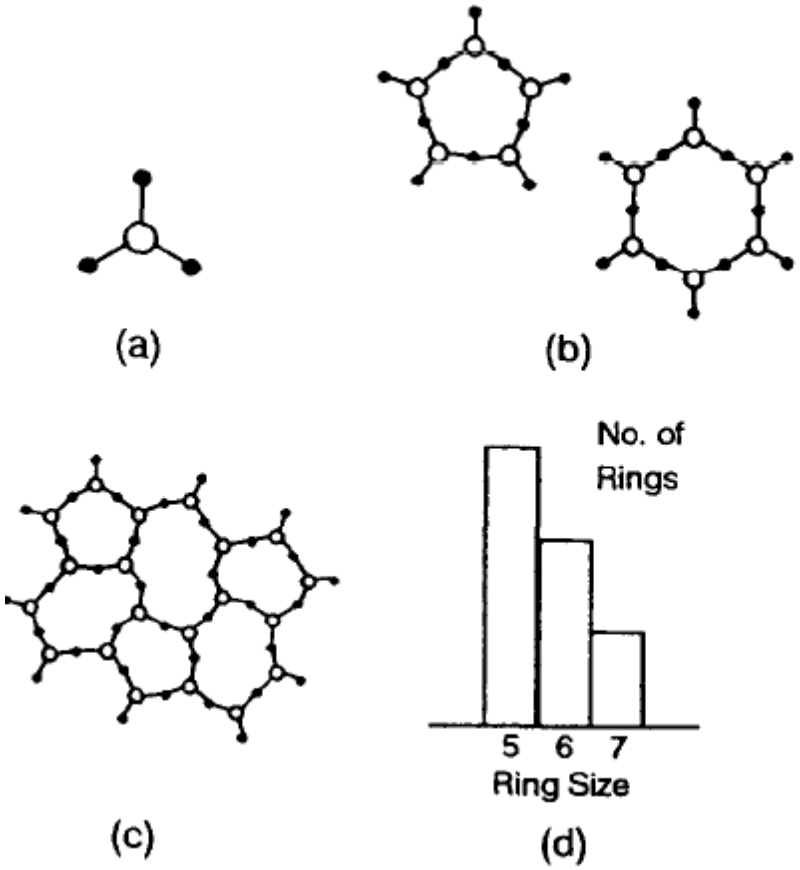

Fig. 1. (a) Triangular cluster of four atoms from a covalent A_2B_3-type amorphous material, (b) rings formed from groups of such clusters, (c) Zachariasen schematic of a 2D CRN comprised of diverse sized rings, and (d) corresponding ring statistics.

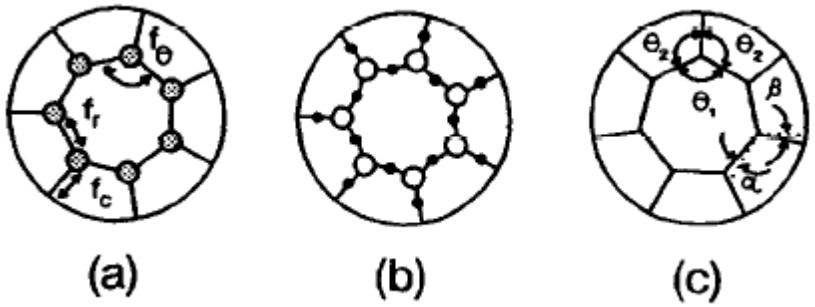

Fig. 2. Structural model for the embedded ring approach for a 2D amorphous material with (a) monatomic composition and (b) polyatomic composition. The three force constants used are indicated schematically in (a). (c) The internal coordinate system for the valence force model.

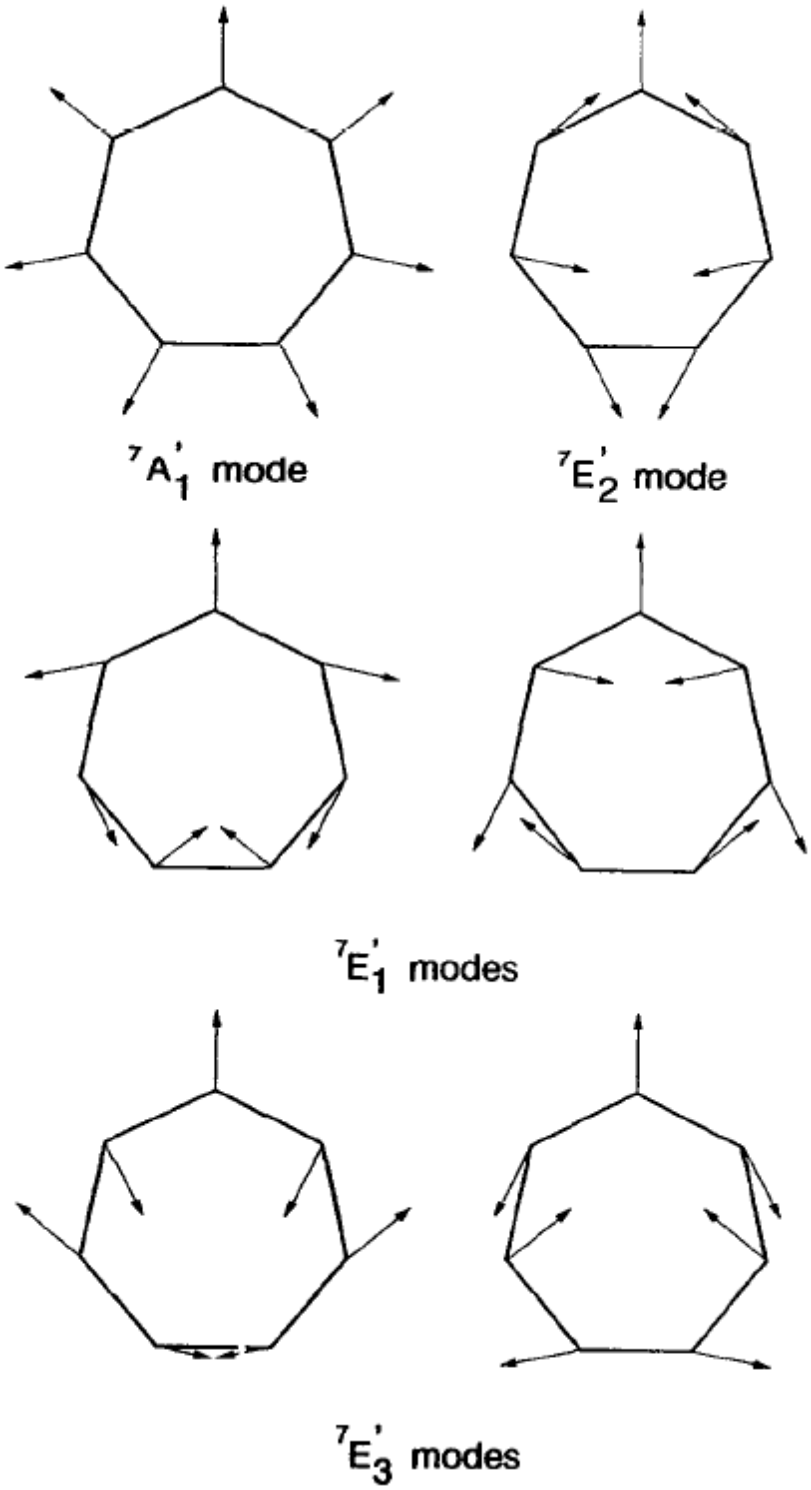

Fig. 3. Fundamental in-plane modes of oscillation for the 7-membered ring.

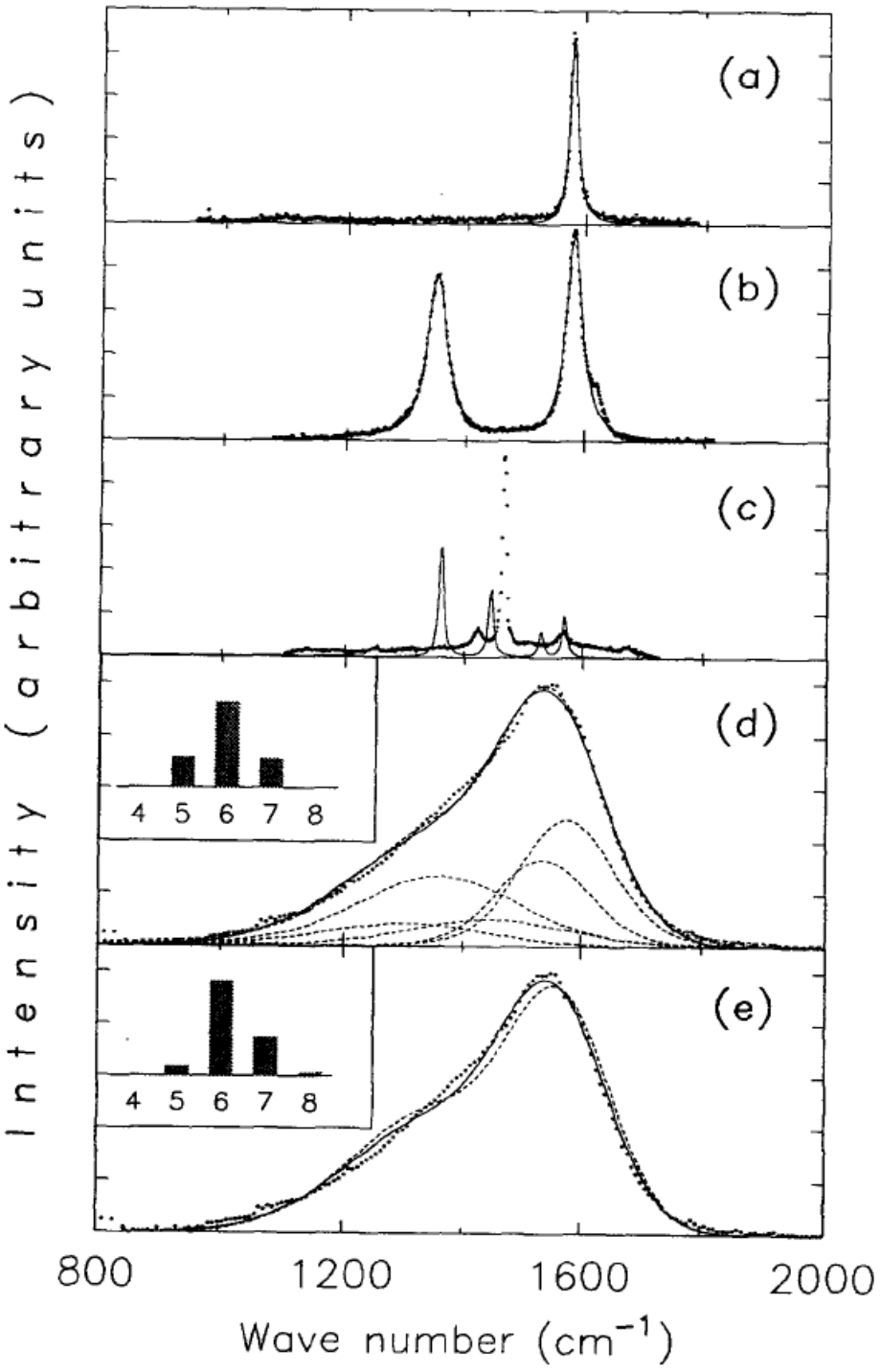

Fig. 4 First-order Raman spectra of (a) graphite, (b) nanocrystalline graphite, (c) C_{60} (d) quasi-2D CRN model of evaporated (graphitic) amorphous carbon, and (e) negative curvature random schwarzite model of amorphous carbon. Curves show least-square fits to the data. Fitting parameters are listed in Table 5. Ring statistics are shown in the insets. The solid (fit d) and dashed (fit d') curves in (d) use Gaussian and convolved Gaussian/Lorentzian lineshapes, respectively. Contributions from each component Gaussian/Lorentzian peak (dashed curves) are also shown in (d). Solid (fit e) and dashed (fit e') curves in (e) use Gaussian/Lorentzian lineshapes with bond lengths t=1.46 Å and t=1.42 Å, respectively.

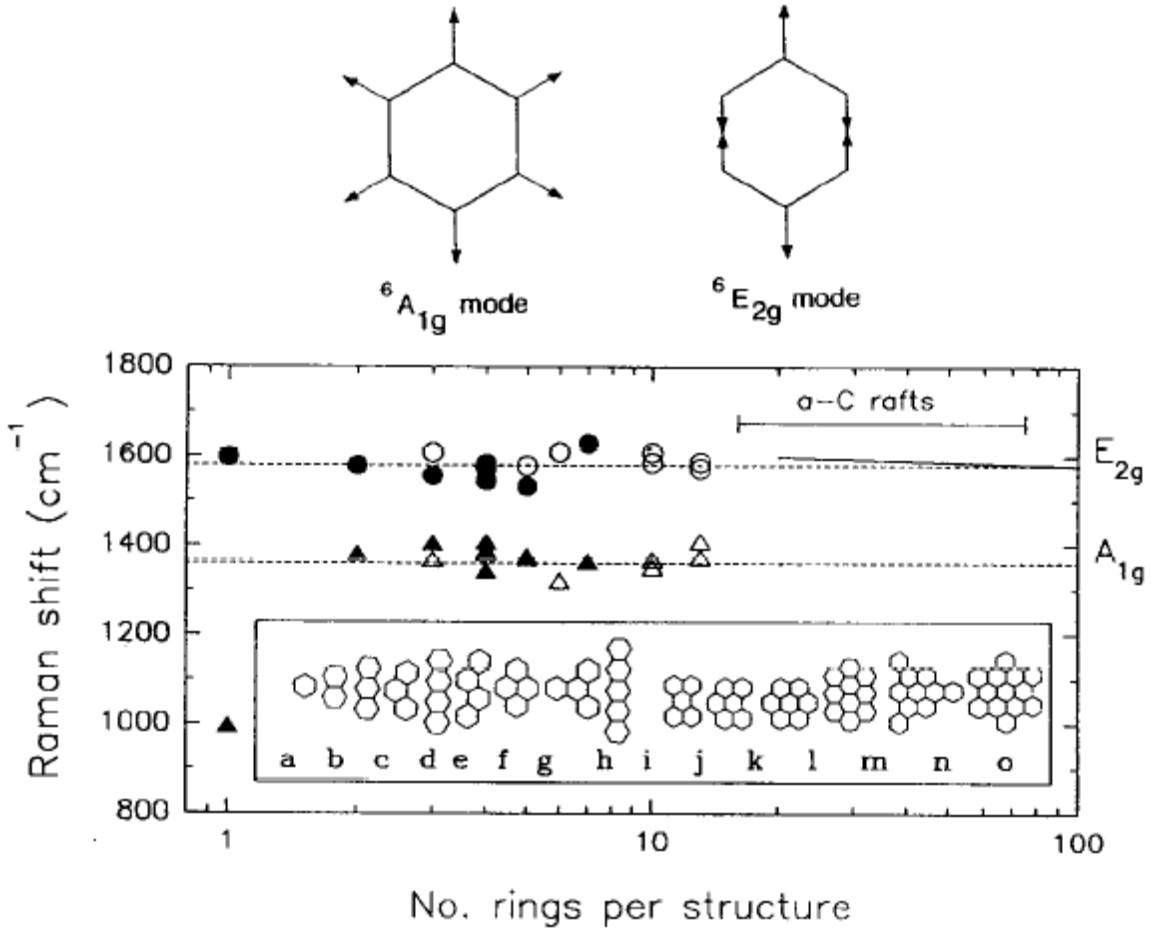

Fig. 5 (Top) In-plane A_{1g} and E_{2g} modes of oscillation of 6-membered embedded rings. These are the only Raman active modes of an isolated 6-membered ring. (Bottom) E_{2g}-like (circles) and A_{1g}-like (triangles) mode frequencies of polycyclic aromatic hydrocarbons versus number of 6-membered rings. Filled symbols indicate that cartesian displacement diagrams were available to aid in assignment of the modes; assignment for the open symbols is somewhat less certain. Molecular structures are shown in the inset: (a) benzene [38], (b) napthalene [38,39], (c) anthracene [38,39], (d) phenanthrene [39], (e) tetracene [38], (f) chrysene [40a], (g) pyrene [38,39,40d], (h) triphenylene [38,40b], (i) pentacene [38], (j) perylene [38,40d], (k) benzo(g,h,i)perylene [38,40c], (l) coronene [38,39], (m) ovalene [38], (n) tribenzo(a,g,m)coronene [41], (o) hexobenzocoronene-A [37], and hexobenzocoronene-B [37]. The dashed lines show the frequencies of the E_{2g} and A_{1g} modes in large nanocrystalline graphite; the solid line indicates the frequency change with domain size of these modes [31]. The range of the number of rings (. 15-75) in 10 Å to 20 Å diameter amorphous carbon rafts is also indicated.

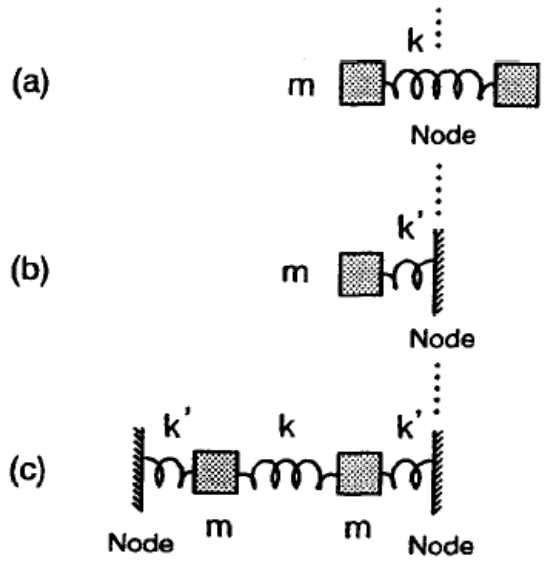

Fig. 6. Two mass-spring system (a), rigid wall-mass-spring system (b), and embedded mass-spring system (c) used to illustrate the coupling force constant and loss of degeneracy in the embedded ring system.

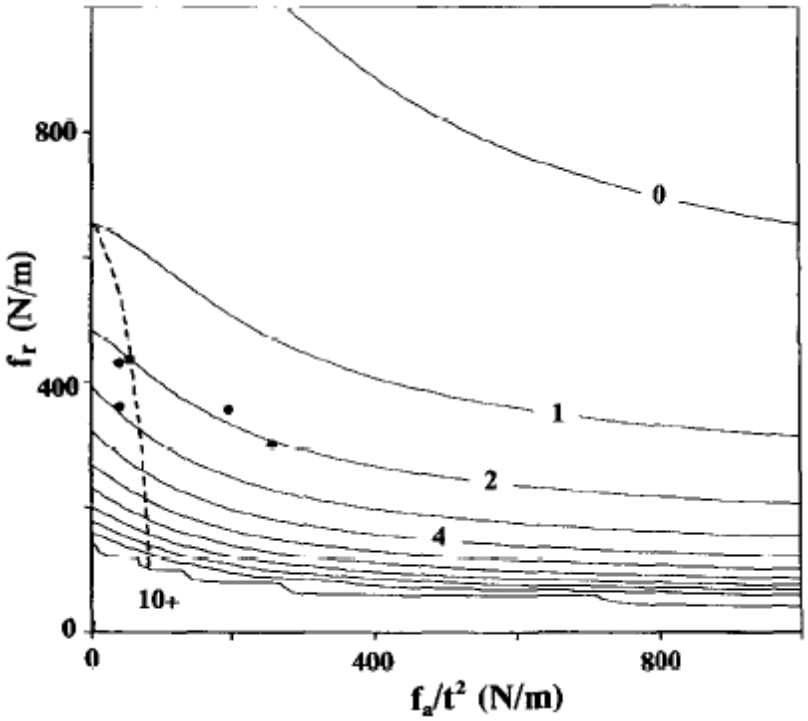

Fig. 7. Dependence of the ratio of the coupling force constant to the bond-stretching force constant, $\eta / f_c/f_r$, on the values of bond-angle bending constant, f_Θ/t^2 and bond-stretching force constant, f_r, when constrained to match the experimental frequencies of nanocrystalline graphite. The dashed line indicates the values subject to the additional constraint, $f_c=\eta f_r$. The symbol, ■, corresponds to the values when $f_c=2f_r$. The symbols, ●, represent values of f_Θ/t^2 and f_r cited in the literature [24,44].

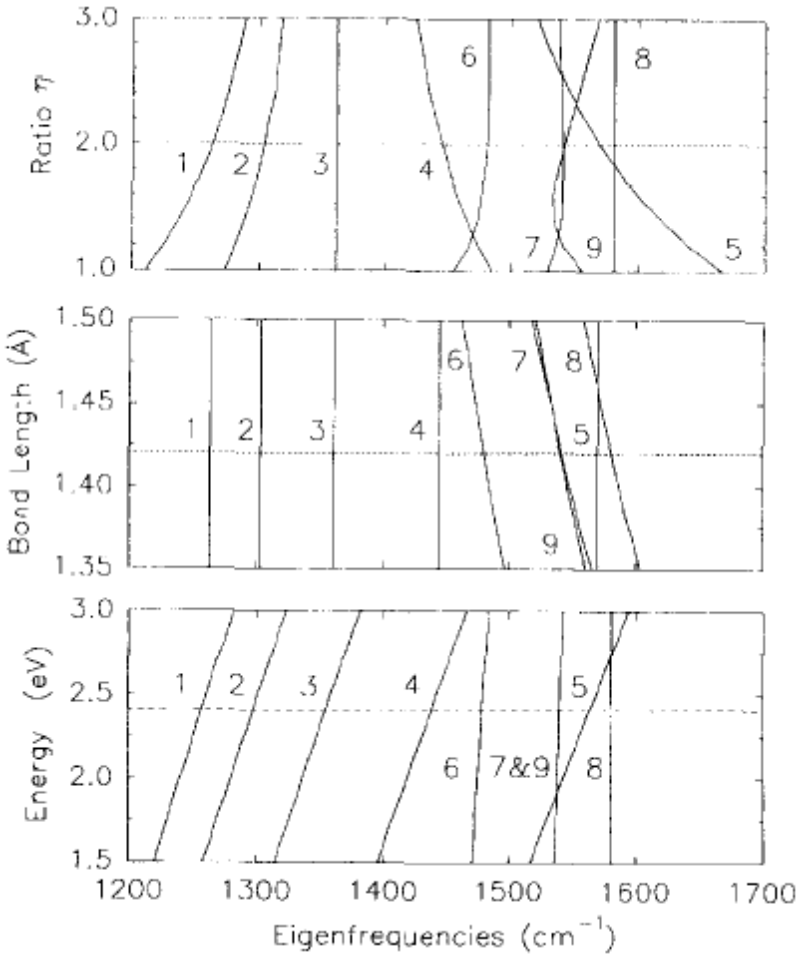

Fig. 8. Eigenfrequencies ω of the A_1- and E_2-type modes for n=4,5,6,7 and 8 as a function of (a) the force constant ratio η, (b) the bond length t, and (c) the Raman excitation laser energy. The horizontal lines indicate the values listed in Table 4. The frequency curves are denoted as follows: 1-$^8A_{1g}$, 2-$^7A_{1'}$, 3-$^6A_{1g}$, 4-$^5A_{1'}$, 5-$^4A_{1g}$, 6-$^8E_{2g}$, 7-$^7E_{2'}$, 8-$^6E_{2g}$, and 9-$^5E_{2'}$.

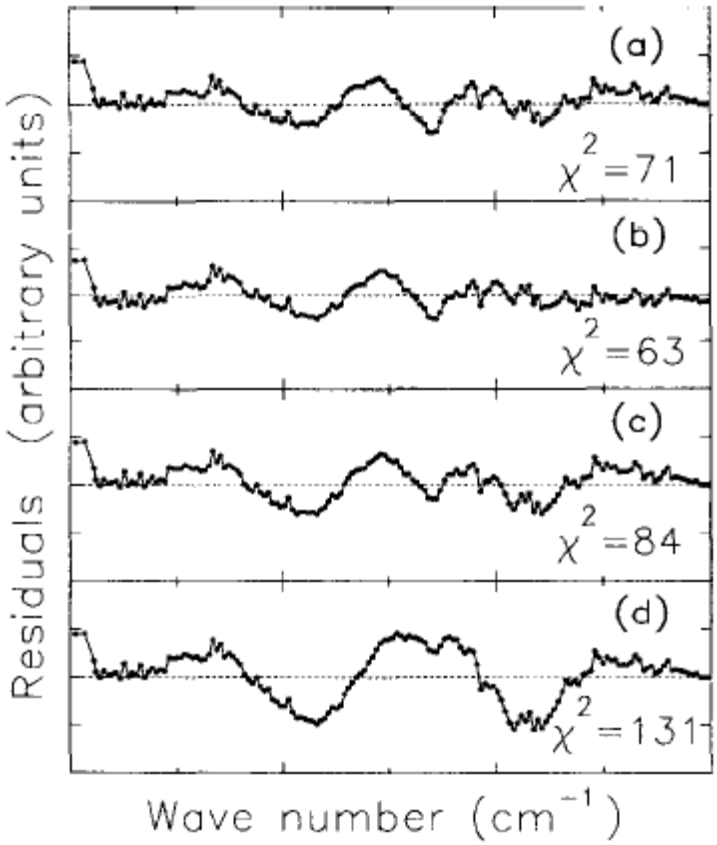

Fig. 9 Residuals of the fits to Raman spectrum of graphitic amorphous carbon based on (a) fit *d*, (b) fit *d'*, (c) fit *e* and (d) fit *e'* , as listed in Table 5 and plotted in Figs. 4(d) and 4(e).

Table 1. Embedded ring vibrational species: In-plane, fundamental, and Raman active modes.

Ring size	In-plane modes	Fundamental modes	Raman active modes
4	A_{1g}, A_{2g}, B_{1g}, B_{2g}, E_{1u}	$\Gamma_{\text{in-plane}} = A_{1g} + B_{1g} + B_{2g} + E_{1u}$	A_{1g}, B_{1g}, B_{2g}
5	A_1N, A_2N, E_1N, E_2N	$\Gamma_{\text{in-plane}} = A_1N + E_1N + 2\,E_2N$	A_1N, E_2N
6	A_{1g}, A_{2g}, B_{1u}, B_{2u}, E_{1u}, E_{2g}	$\Gamma_{\text{in-plane}} = A_{1g} + B_{1u} + B_{2u} + E_{1u} + 2\,E_{2g}$	A_{1g}, E_{2g}
7	A_1N, A_2N, E_1N, E_2N, E_3N	$\Gamma_{\text{in-plane}} = A_1N + E_1N + 2\,E_2N + 2\,E_3N$	A_1N, E_2N
8	A_{1g}, A_{2g}, B_{1g}, B_{2g}, E_{1u}, E_{3u}, E_{2g}	$\Gamma_{\text{in-plane}} = A_{1g} + B_{1g} + B_{2g} + E_{1u} + 2\,E_{3u} + 2\,E_{2g}$	A_{1g}, E_{2g}

Table 2. Symmetry coordinates for in-plane fundamental modes of n-membered rings.

$^{n}B_1$ type modes

$$\tfrac{1}{2}\sum_{k=1}^{n} t_k,\quad \tfrac{1}{2}\sum_{k=1}^{n} s_k,\quad \tfrac{1}{2}\sum_{k=1}^{n} \alpha_k \qquad \tfrac{1}{2}\sum_{k=1}^{n} (-1)^{k-1} s_k,\quad \tfrac{1}{2}\sum_{k=1}^{n} (-1)^{k-1} \alpha_k \qquad \tfrac{1}{2}\sum_{k=1}^{n} (-1)^{k-1} t_k,\quad \tfrac{1}{2}\sum_{k=1}^{n} (-1)^{k-1} \beta_k$$

$^{n}A_1$-type modes

$^{n}B_2$-type modes

$^{n}E_j$-type modes

$$\sqrt{\frac{2}{n}}\sum_{k=1}^{n} \cos\left[\frac{2\pi}{n} j\,(k\text{-}\tfrac{1}{2})\right] t_k \qquad \sqrt{\frac{2}{n}}\sum_{k=1}^{n} \cos\left[\frac{2\pi}{n} j\,(k\text{-}1)\right] s_k$$

$$\sqrt{\frac{2}{n}}\sum_{k=1}^{n} \cos\left[\frac{2\pi}{n} j\,(k\text{-}1)\right] \alpha_k \qquad \sqrt{\frac{2}{n}}\sum_{k=1}^{n} \sin\left[\frac{2\pi}{n} j\,(k\text{-}1)\right] \beta_k$$

Table 3(a). F- and G-matrices for $^{n}A_1$-, $^{n}B_1$-, $^{n}B_2$-, and $^{n}E_j$-type modes, where f_c is the coupling force constant, f_r is the bond-stretching force constant, and f_Θ is the bond-angle-bending force constant. Asterisks are redundant elements.

$^{n}A_1$-type mode

$$\begin{bmatrix} f_c & 0 \\ 0 & f_b \end{bmatrix} \qquad \begin{bmatrix} g_{ss}^{2} & 2\,g_{st}^{1} \\ * & g_{tt}^{2} + g_{tt}^{1} \end{bmatrix}$$

$^{n}B_1$-type mode

$$\begin{bmatrix} f_c & 0 \\ 0 & f_a \end{bmatrix} \qquad \begin{bmatrix} g_{ss}^{2} & g_{s\alpha}^{1}\left(\begin{smallmatrix}1\\1\end{smallmatrix}\right) - 2\,g_{s\alpha}^{1}\left(\begin{smallmatrix}1\\1\end{smallmatrix}\right) \\ * & g_{\alpha\alpha}^{3} + g_{\alpha\alpha}^{2}\left(\begin{smallmatrix}1\\0\end{smallmatrix}\right) + 2\,g_{\alpha\alpha}^{1}\left(\begin{smallmatrix}2\\2\end{smallmatrix}\right) \end{bmatrix}$$

$^{n}B_2$-type mode

$$\begin{bmatrix} f_b & 0 \\ 0 & f_a \end{bmatrix} \qquad \begin{bmatrix} g_{tt}^{2} - 2\,g_{tt}^{1} & 2\left[g_{t\beta}^{1}\left(\begin{smallmatrix}1\\1\end{smallmatrix}\right) + g_{t\beta}^{1}\left(\begin{smallmatrix}1\\2\end{smallmatrix}\right)\right] \\ * & g_{\beta\beta}^{3} - 2\,g_{\beta\beta}^{2}\left(\begin{smallmatrix}1\\0\end{smallmatrix}\right) + 2\,g_{\beta\beta}^{1}\left(\begin{smallmatrix}2\\2\end{smallmatrix}\right) \end{bmatrix}$$

$^{n}E_j$-type mode

$$\begin{bmatrix} f_c & 0 & 0 & 0 \\ 0 & f_b & 0 & 0 \\ 0 & 0 & f_a & 0 \\ 0 & 0 & 0 & f_a \end{bmatrix} \qquad \begin{bmatrix} g_{ss}^{2} & -C_1 g_{st}^{1} & g_{s\alpha}^{1}\left(\begin{smallmatrix}1\\1\end{smallmatrix}\right) + C_2 g_{s\alpha}^{1}\left(\begin{smallmatrix}1\\2\end{smallmatrix}\right) & S_2 g_{s\beta}^{1}\left(\begin{smallmatrix}1\\2\end{smallmatrix}\right) \\ * & g_{tt}^{2} + C_2 g_{tt}^{1} & C_1 g_{t\alpha}^{2} + C_3 g_{t\alpha}^{1}\left(\begin{smallmatrix}1\\2\end{smallmatrix}\right) & -S_1 g_{t\beta}^{1}\left(\begin{smallmatrix}1\\1\end{smallmatrix}\right) + S_3 g_{t\beta}^{1}\left(\begin{smallmatrix}1\\2\end{smallmatrix}\right) \\ * & * & g_{\alpha\alpha}^{3} + C_2 g_{\alpha\alpha}^{2}\left(\begin{smallmatrix}1\\0\end{smallmatrix}\right) + C_4 g_{\alpha\alpha}^{1}\left(\begin{smallmatrix}2\\2\end{smallmatrix}\right) & S_3 g_{\alpha\beta}^{1}\left(\begin{smallmatrix}2\\2\end{smallmatrix}\right) + S_4 g_{\alpha\beta}^{1}\left(\begin{smallmatrix}2\\1\end{smallmatrix}\right) \\ * & * & * & g_{\beta\beta}^{3} + C_2 g_{\beta\beta}^{2}\left(\begin{smallmatrix}1\\0\end{smallmatrix}\right) + C_4 g_{\beta\beta}^{1}\left(\begin{smallmatrix}2\\2\end{smallmatrix}\right) \end{bmatrix}$$

where $C_k = 2\cos\left(\frac{jk}{n}\pi\right)$

and $S_k = 2\sin\left(\frac{jk}{n}\pi\right)$

with $j = 1,2,3$; $k = 1...4$; $n = 4...8$.

Table 3(b). Generalized g-matrix elements used in the embedded ring approach for n-membered rings (n=4, 5, 6, 7, 8) in terms of internal coordinates. In the expressions μ is the reciprocal mass of the ring atom, τ/t^{-1} is the reciprocal atom-atom bond length, σ/s^{-1} is the reciprocal atom-rigid wall distance, $\theta^n_1/[(n-2)/n]\pi$ is the ring's inner bond angle, and $\theta^n_2/[(n+2)/2n]\pi$ is the angle between the coupling bond and atom-atom bond [see Fig. 2(c)].

$$g^2_{zz}=\mu \qquad g^1_{x\alpha}\left(\tfrac{1}{2}\right)=\tau\mu\sin\theta^n_1 \qquad g^1_{x\alpha}\left(\tfrac{1}{1}\right)=-2\tau\mu\cos\theta^n_2\left[\frac{1-\cos\theta^n_1}{\sin\theta^n_1}\right] \qquad g^3_{\beta\beta}=\mu\left[\sigma^2+2\sigma\tau\cos\tfrac{1}{2}\theta^n_1+\tau^2\left(\tfrac{1}{2}+\cos^2(\tfrac{1}{2}\theta^n_1)\right)\right]$$

$$g^2_{xx}=2\mu \qquad g^3_{\alpha\alpha}=2\tau^2\mu\left[2-\cos\theta^n_1\right] \qquad g^1_{x\alpha}\left(\tfrac{1}{2}\right)=-\tau\mu\sin\theta^n_2 \qquad g^2_{\beta\beta}\left(\tfrac{1}{0}\right)=\tau\mu\cos\tfrac{1}{2}\theta^n_1\left[\sigma+\tau\cos\tfrac{1}{2}\theta^n_1\right]$$

$$g^1_{xx}=\mu\cos\theta^n_1 \qquad g^2_{\alpha\alpha}\left(\tfrac{1}{0}\right)=-2\tau^2\mu\left[1-\cos\theta^n_1\right] \qquad g^1_{x\beta}\left(\tfrac{1}{1}\right)=\mu\left[\sigma\sin\tfrac{1}{2}\theta^n_1+\tfrac{1}{2}\tau\sin\theta^n_1\right] \qquad g^1_{\beta\beta}\left(\tfrac{2}{2}\right)=\tfrac{1}{4}\tau^2\mu\cos\theta^n_1$$

$$g^1_{xx}=\mu\cos\theta^n_2 \qquad g^1_{\alpha\alpha}\left(\tfrac{2}{2}\right)=-\tau^2\mu\cos\theta^n_1 \qquad g^1_{x\beta}\left(\tfrac{1}{2}\right)=-\tfrac{1}{2}\tau\mu\sin\theta^n_1 \qquad g^1_{\alpha\beta}\left(\tfrac{2}{2}\right)=-\tfrac{1}{2}\tau^2\mu\cos\theta^n_1$$

$$g^2_{xx}=-\tau\mu\sin\theta \qquad g^1_{x\beta}\left(\tfrac{1}{2}\right)=\tfrac{1}{2}\tau\mu\sin\tfrac{1}{2}\theta^n_1 \qquad g^1_{\alpha\beta}\left(\tfrac{2}{1}\right)=-\tau\mu\left[\tau+\sigma\cos\tfrac{1}{2}\theta^n_1\right]$$

Table. Secular equations for n-membered rings

$$\text{"}A_1\text{-type modes:}\quad -4f_bf_c\mu^2\cos^2\theta^n_2+2f_b\mu\left(f_c\mu-\omega^2\right)\cos\theta^n_1+\left(f_c\mu-\omega^2\right)\left(2f_b\mu-\omega^2\right)$$

$$\text{"}B_1\text{-type modes:}\quad -4f_af_c\tau^2\mu^2\left[\cos\theta^n_2\frac{\left(\cos\theta^n_1-1\right)}{\sin\theta^n_1}-\sin\theta^n_2\right]^2+8f_a\tau^2\mu\cos\theta^n_1\left(\omega^2-f_c\mu\right)+\left(f_c\mu-\omega^2\right)\left(8f_a\tau^2\mu-\omega^2\right)$$

$$\text{"}B_2\text{-type modes:}\quad \mu\left(2f_b\cos\theta^n_1-f_a\sigma^2\right)\omega^2+\omega^2\left(\omega^2-2f_b\mu\right)$$

Table 4. Fundamental, in-plane mode frequencies for graphitic amorphous carbon determined with the embedded ring approach, using f_r=436 N/m, f_Θ/t_2=55 N/m and $f_c=2f_r$ with t=1.42 Å. Raman active modes of isolated, planar, symmetric rings are shown in italics.

n	Eigenfrequency (cm^{-1})					
4	***A_{1g} (1570)***	***B_{1g} (1363)***	***B_{2g} (1145)***	E_{1u} (714,1592)		
5	***A_1N (1444)***			E_1N (704,1529)	***E_2N (1103,1542)***	
6	***A_{1g} (1360)***	B_{1u} (1473)	B_{2u} (1388)	E_{1u} (684,1446)	***E_{2g} (1013,1581)***	
7	***A_1N (1303)***			E_1N (659,1375)	***E_2N (947,1541)***	E_3N (1318,1563)
8	***A_{1g} (1263)***	B_{1g} (1516)	B_{2g} (1477)	E_{1u} (633,1320)	***E_{2g} (897,1480)***	E_{3u} (1225,1584)

Table 5. Fitting parameters for Raman spectra of graphitic carbon.

Fit	Material	Bond Length t	Force constants f_r and f_Θ/t^2 [a]	Ring statistics % n={4,5,6,7,8}	C_A/C_E	Peak widths (cm^{-1})
a	Graphite	1.42 Å	436 N/m, 55 N/m	{0,0,100,0,0}	0	Γ_E=8.1*
b	Nanocryst. Graphite	1.42 Å	436 N/m, 55 N/m	{0,0,100,0,0}	1.27*	Γ_E=16.5*, Γ_A=20.7*
c	C_{60}	1.42 Å [b]	436 N/m, 55 N/m	{0,38,62,0,0}	1.0	Γ=5.0
d	Amorphous Carbon[c]	1.463 Å*	436 N/m, 52 N/m	{0,21,59,20,0}	1.13*	σ_E=85.3*, σ_A=147.8*
d'		1.461 Å*	436 N/m, 52 N/m	{0,21,59,20,0}	1.06*	σ_E=74.0*,Γ_E=16.5, σ_A=130.6*,Γ_A=20.7
e	Random Schwarzite[d]	1.46 Å [d]	436 N/m, 52 N/m	{0,6,66,26,2}	0.95*	σ_E=74.3*,Γ_E=16.5, σ_A=127.8*,Γ_A=20.7
e'		1.42 Å	436 N/m, 55 N/m	{0,6,66,26,2}	0.94*	σ_E=71.5*,Γ_E=16.5, σ_A=130.6*,Γ_A=20.7

*Adjustable fitting parameters. [a] All calculations used $f_c=2f_r$. [b] Ref. 47. [c] Ref. 24. [d] Ref. 48.